Available online at www.sciencedirect.com

SciVerse ScienceDirect

Ceramics International 39 (2013) 3539–3545

CERAMICS INTERNATIONAL

www.elsevier.com/locate/ceramint

Enhanced NO_2 sensing properties of Zn_2SnO_4-core/ZnO-shell nanorod sensors

Sunghoon Park, Soyeon An, Hyunsung Ko, Changhyun Jin, Chongmu Lee*

Department of Materials Science and Engineering, Inha University, 253 Yonghyun-dong, Nam-gu, Incheon 402-751, Republic of Korea

Received 24 July 2012; received in revised form 17 September 2012; accepted 8 October 2012
Available online 16 October 2012

Abstract

Zn_2SnO_4-core/ZnO-shell nanorods were synthesized using a two-step process: synthesis of Zn_2SnO_4 nanorods the thermal evaporation of a mixture of ZnO, SnO_2, and graphite powders, followed by atomic layer deposition (ALD) of ZnO. The nanorods were 50–250 nm in diameter and a few to a few tens of micrometers in length. The cores and shells of the nanorods were face-centered cubic-structured single crystal Zn_2SnO_4 and wurtzite-structured single crystal ZnO, respectively. The multiple networked Zn_2SnO_4-core/ZnO-shell nanorod sensors showed a response of 173–498% to NO_2 concentrations of 1–5 ppm at 300 °C. These response values are 2–5 times higher than those of the Zn_2SnO_4 nanorod sensor over the same NO_2 concentration range. The NO_2 sensing mechanism of the Zn_2SnO_4core/ZnO-shell nanorods is discussed.
Crown Copyright © 2012 Published by Elsevier Ltd and Techna Group S.r.l. All rights reserved.

Keywords: Zn_2SnO_4 nanorods; ZnO shells; Gas sensors; NO_2

1. Introduction

One-dimensional (1D) nanostructure-based sensors have higher sensitivity, superior spatial resolution and rapid response compared to thin film gas sensors due to the high surface-to-volume ratios of individual nanowires [1,2]. Therefore, considerable has been devoted to the synthesis of 1D MOS nanostructures including SnO_2, ZnO, TiO_2 and In_2O_3 [3–6]. Nevertheless, enhancing their sensing performance and detection limit is a still challenge. The heterogeneous interface between oxide semiconductors was proposed to enhance the sensitivity, stability, and response speed of 1D nanostructure-based sensors. Mixture- [7–9] and layered-type [10–12] composite sensors were also proposed to improve the stability of the interface.

On the other hand, zinc stannate has high electron mobility, high electrical conductivity and low visible absorption, which makes it suitable for a wide range of applications, such as solar cells and sensors for humidity and combustible gases [13–17]. Recently, a range of techniques including thermal evaporation, high-temperature calcination, mechanical grinding, sol–gel synthesis, hydrothermal reactions, and ion-exchange reactions have been used to synthesize zinc stannate 1D nanostructures [18]. Zinc stannate, during crystallization through a solid-state reaction, normally transforms through a metastable form ($ZnSnO_3$) at temperatures of 300–500 °C to the stable zinc orthostannate (Zn_2SnO_4) at temperatures above 600 °C. A pure Zn_2SnO_4 phase is difficult to obtain using high-temperature synthesis methods, such as thermal evaporation, with the end product normally being a mixed phase of $ZnSnO_3$, Zn_2SnO_4 and SnO_2 [18]. Metastable $ZnSnO_3$ has a face-centered perovskite structure, whereas the orthostable Zn_2SnO_4 has a cubic spinel structure [19].

Over the past two decades, Zn_2SnO_4 1D nanostructures have attracted interest for sensing *i*-C_4H_{10} [20], NO [21], NO_2 [22], C_2H_5OH [23], and CO gases [24]. In addition, heterostructure formation techniques have been developed to enhance the sensing performance, detection limit and operation temperature of sensors comprised of 1D nanostructures [25–29]. On the other hands, there is little literature the sensing properties of Zn_2SnO_4 based 1D

*Corresponding author. Tel.: +82 32 860 7536; fax: +82 32 862 5546.
E-mail address: cmlee@inha.ac.kr (C. Lee).

0272-8842/$ - see front matter Crown Copyright © 2012 Published by Elsevier Ltd and Techna Group S.r.l. All rights reserved.
http://dx.doi.org/10.1016/j.ceramint.2012.10.178

nanoheterostructures This paper, reports the enhanced sensing properties of Zn_2SnO_4-core/ZnO-shell nanorods for detecting NO_2 gas.

2. Experimental

The Zn_2SnO_4-core/ZnO-shell nanorods were synthesized using a two-step process: synthesis of Zn_2SnO_4 nanorods by the thermal evaporation of a mixture of ZnO, SnO_2, and graphite powders (2: 1: 3 wt%) followed by atomic layer deposition (ALD) of ZnO. Zn_2SnO_4 nanorods were synthesized on Au-coated c-plane sapphire (Al_2O_3) substrates by thermal evaporation. Approximately 1.5 g of a mixture of ZnO, SnO_2 and graphite powders (ZnO: SnO_2: graphite = 2: 1: 3 in weight ratio) used as the starting materials was placed in an alumina crucible and positioned at the center of a horizontal quartz tube. The quartz tube was mounted inside a conventional horizontal tube furnace. During nanorods synthesis, the temperature of the source materials was maintained at 1000 °C for 1 h, whereas that of the sapphire substrates was maintained at 700 °C in an Ar/O_2 atmosphere at Ar and O_2 flow rates of 95 and 5 sccm, respectively. The pressure in the reactor was kept at 1 Torr. After the synthesis process, the furnace was cooled to room temperature and the sapphire substrate was removed from the tube. Subsequently, Zn_2SnO_4 nanorods were transferred to an ALD chamber. The nanorods were coated with ZnO. Diethylzinc (DEZn) and H_2O were kept in bubblers at 0 °C and 10 °C, respectively. These source gases were fed alternatively into the chamber through separate inlet lines and nozzles. The typical pulse lengths were 0.15 s for DEZn (0 °C), 0.2 s for H_2O (10 °C) and 3 s for purging the reactants. The substrate temperature and pressure in the chamber were 150 °C and 0.1 Torr, respectively.

The collected nanorod samples were characterized by scanning electron microscopy (SEM, Hitachi S-4200), transmission electron microscopy (TEM, Philips CM-200) equipped with an energy-dispersive X-ray spectrometer (EDXS) and X-ray diffraction (XRD, Philips X'pert MRD diffractometer). The crystallographic structure was determined by glancing angle XRD using Cu K_α radiation (0.15406 nm) at a scan rate of 2 °/min. The sample was arranged geometrically at a 0.5° glancing angle with a rotating detector.

For the sensing measurments, Ni (~10 nm in thickness) and Au (~50 nm) thin films were deposited sequentially by sputtering to form electrodes using an interdigital electrode (IDE) mask. Multiple networked Zn_2SnO_4-core/ZnO-shell nanorod gas sensors were fabricated by pouring a few drops of nanorod-suspended ethanol onto oxidized Si substrates equipped with a pair of IDEs and a gap length of 20 μm. The electrical and gas sensing properties of the as-synthesized Zn_2SnO_4 nanorods and Zn_2SnO_4-core/ZnO-shell nanorods were measured using a home-built computer-controlled characterization system consisting of a test chamber, sensor holder, Keithley sourcemeter-2612, mass flow controllers and a data acquisition system (Fig. 1). During the measurements, the nanorod gas sensors were placed in a sealed quartz tube with an electrical feed through. The test gas was mixed with dry air to achieve the desired concentration, and the flow rate was maintained at 200 sccm using mass flow controllers. The current flowing through the samples was measured using a Keithley sourcemeter-2612. The working temperature of the sensors was adjusted by changing the voltage across the heater side. The gas sensing properties of the Zn_2SnO_4-core/ZnO-shell nanorods were measured at 300 °C in a quartz tube placed in a sealed chamber with an electrical feed through. A given amount of NO_2 (> 99.99%, 1–5 ppm) gas was injected into the testing tube through a microsyringe, and the output voltage across the sensor in the nanotubes was monitored. The resistance of the sensor in dry air or in the test gas was measured from this voltage. The response of the Zn_2SnO_4 nanorods sensors is defined as R_g/R_a for NO_2, where R_a and R_g are the electrical currents in the sensors in air and target gas, respectively. The response time is defined as the time required for the change in electrical current to reach 90% of the equilibrium value after injecting the gas. The recovery time is defined as the time needed for the sensor to return to 90% of the original current in air after removing the gas.

3. Results and discussion

Fig. 2 shows a SEM image of the Zn_2SnO_4-core/ZnO-shell nanorods prepared by thermal evaporation followed by ALD. SEM showed that the synthesis scheme adopted in this study can grow ZnO nanorods with diameters of 50–250 nm and lengths of a few to a few tens of micrometers.

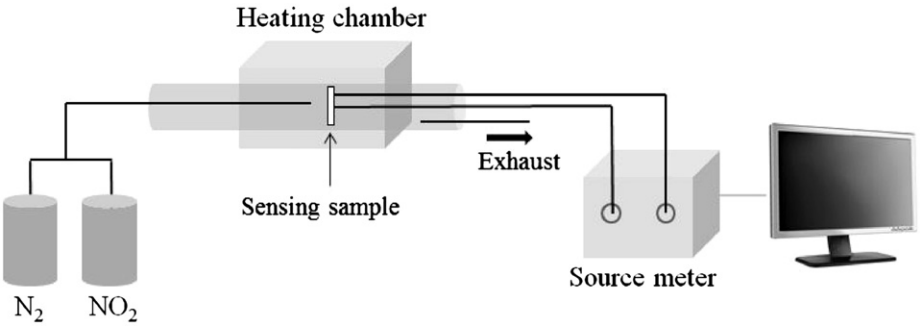

Fig. 1. Schematic diagram of the home-built computer-controlled characterization system.

The globular particle at the tip of a typical core-shell nanorod in the enlarged SEM image (Fig. 2, inset) suggests that the nanorod was grown using a VLS (Vapor–Liquid–Solid) mechanism. The low-magnification TEM image of a typical core-shell nanorod revealed a Zn_2SnO_4 core with a diameter of ~120 nm at the central region and ZnO shells with a width of ~20 nm at the two edge regions of the nanorod (Fig. 3(a)). The enlarged high resolution TEM (HRTEM) image shows the fringe patterns in the two different regions, suggesting both the core and shell are single crystals. The resolved spacings between the two parallel neighboring fringes were 0.26, 0.18, and 0.19 nm, corresponding to the interplanar distances of the {311} and {422} lattice planes in fcc Zn_2SnO_4 and the {1 0 2} lattice planes in wurtzite ZnO, respectively (Fig. 3(b)). The spotty patterns in the corresponding selected area electron diffraction (SAED) pattern confirmed both the Zn_2SnO_4 core and ZnO shell to be single crystals.

The XRD patterns of the Zn_2SnO_4 nanorods and Zn_2SnO_4-core/ZnO-shell nanorods also confirmed that both the Zn_2SnO_4 cores and ZnO shells were single crystals (Fig. 4). The XRD peaks of the Zn_2SnO_4 nanorods were assigned to the (220), (311), (222), (400), (422), (511), (440), (442), (533) and (444) planes of fcc-structured Zn_2SnO_4 with lattice constants of $a=0.865$ nm (JCPDS no. 74-2184). On the other hand, the peaks in the XRD pattern of the core-shell nanorods were assigned to the (102) and (004) planes of wurtzite-type hexagonal-structured ZnO with lattice constants of $a=0.3253$ nm and $c=0.5213$ (JCPDS no. 89-1397) along with the reflections from fcc-structured Zn_2SnO_4. EDXS confirmed that the core-shell nanostructures were composed of Zn, Sn and O (Fig. 5(a)). The Cu and C in the spectra were assisted to TEM grid. EDXS suggested that Zn_2SnO_4-core/ZnO-shell nanorods had been synthesized successfully by indicating a higher Sn concentration in the central region and a higher Zn concentration at both edge regions of the nanorod (Fig. 5(b)).

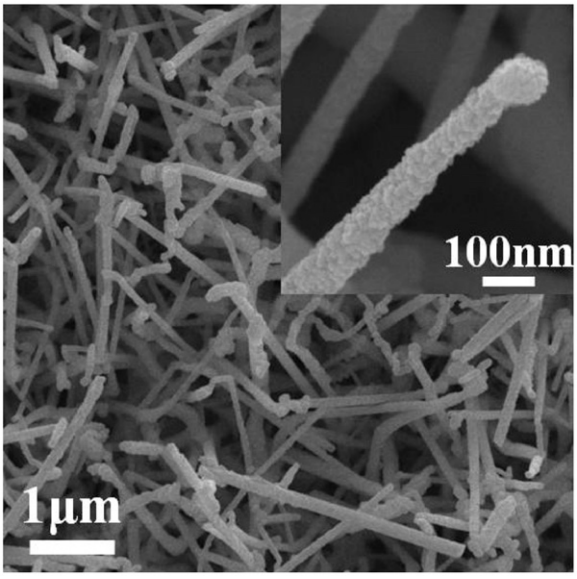

Fig. 2. SEM image of Zn_2SnO_4-core/ZnO-shell nanorods. Inset, enlarged SEM image of a typical core-shell nanorod.

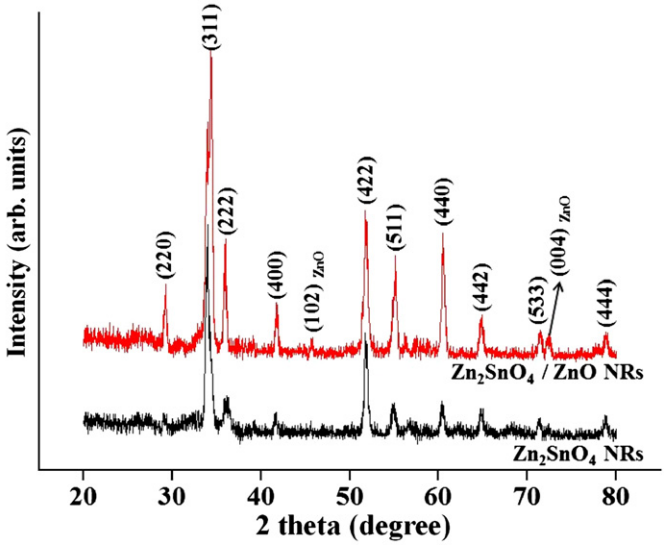

Fig. 4. XRD patterns of ZnO nanorods and Zn_2SnO_4-core/ZnO-shell nanorods.

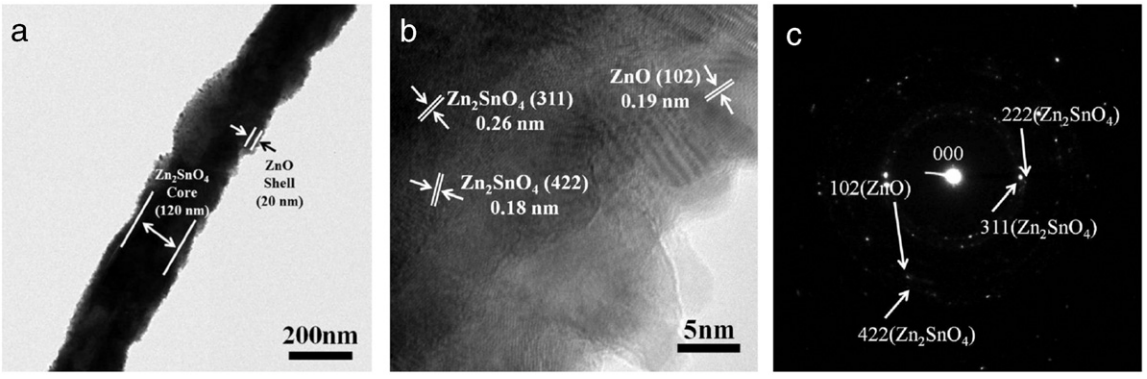

Fig. 3. (a) Low magnification TEM image, (b) high resolution TEM image, and (c) selected area electron diffraction pattern of Zn_2SnO_4-core/ZnO-shell nanorods.

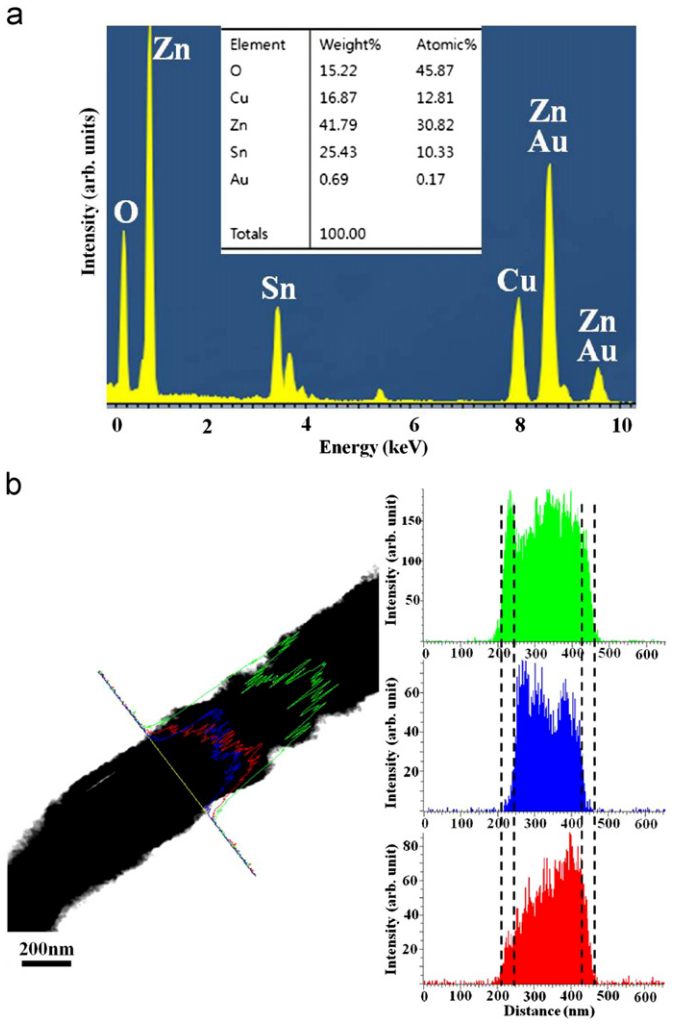

Fig. 5. (a) EDX spectra of the Zn_2SnO_4-core/ZnO-shell nanorods and (b) EDXS line scanning concentration profiles.

Fig. 6(a) shows the dynamic responses of the Zn_2SnO_4 nanorods and Zn_2SnO_4-core/ZnO-shell nanorods at 300 °C to NO_2. The resistance increased upon exposure to NO_2 and recovered completely to the initial value upon the removal of NO_2. The sensor responses to NO_2 gas were also stable and reproducible for repeated test cycles. Fig. 6(b) and (c), shows the enlarged part of the data in Fig. 6(a) measured at a NO_2 concentration of 5 ppm for the Zn_2SnO_4 nanorods and Zn_2SnO_4-core/ZnO-shell nanorods, respectively to reveal the moments of gas input and gas stop. The Zn_2SnO_4 nanorods showed responses of approximately 102, 106, 109, 114 and 118% at NO_2 concentrations of 1, 2, 3, 4 and 5 ppm, respectively (Table 1). On the other hand, ZnO showed responses of approximately 3.84 and 5.56% at NO_2 concentrations of 1 and 5 ppm, respectively (Table 1) [30]. Therefore, the responses of the Zn_2SnO_4 nanorods were significantly higher (~26 and 21 fold) than those of the ZnO nanowires at 1 and 5 ppm NO_2, respectively. In contrast, the Zn_2SnO_4-core/ZnO-shell nanorods showed responses of 173, 240, 341, 397 and 498% at NO_2 concentrations of 1, 2, 3, 4 and 5 ppm, respectively (Table 1). Therefore, the response of the nanorods was increased ~2–5 fold at each NO_2 concentration by the encapsulation of Zn_2SnO_4 nanorods with ZnO, and was ~45 and ~90 fold higher than ZnO nanowires at the NO_2 concentrations of 1 and 5 ppm, respectively. Fig. 6(d) shows the responses of Zn_2SnO_4 nanorods and Zn_2SnO_4-core/ZnO-shell nanorods as a function of the NO_2 concentration. The response of an oxide semiconductor is commonly expressed as $R=A\ [C]^n+B$, where A and B, n and [C] are constants, exponent, and target gas concentration, respectively. Data fitting provided the following equations: $R=4.045\ [C]+97.805$ and $R=80.663\ [C]+87.993$ for the Zn_2SnO_4 nanorod and Zn_2SnO_4-core/ZnO-shell nanorod sensors, respectively. The response of the core-shell nanorod sensor tended to increase more rapidly than that of the bare nanorod sensor as the NO_2 gas concentration was increased, suggesting that the response of the former would be far higher than that of the latter at high NO_2 gas concentrations, such as, at a few thousands ppm NO_2, even though the response of the core-shell nanorods were examined only at NO_2 concentrations of 1–5 ppm. Table 1. also shows that the response and recovery times of the core-shell nanorods were decreased somewhat by encapsulation, regardless of the NO_2 concentration, and were far (~3–8 fold) shorter than those of the ZnO nanowires.

The NO_2 gas sensing mechanism of the Zn_2SnO_4 nanorod sensor can be modeled using the surface-depletion model [31], as shown in Fig. 7. When the Zn_2SnO_4 nanorods are exposed to air, they interacts with oxygen by transferring electrons from the conduction band to the adsorbed oxygen atoms, forming ionic species, such as O^-, O^{2-} and O_2^-, as illustrated below, because the Zn_2SnO_4 conduction band minimum is higher than the chemical potential of O_2 [32].

$$O_2\ (g) \rightarrow O_2\ (ads) \quad (1)$$

$$O_2\ (ads) + e^- \rightarrow O_2^-\ (ads) \quad (2)$$

$$O_2^-\ (ads) + e^- \rightarrow 2O^-\ (ads) \quad (3)$$

$$O^-\ (ads) + e^- \rightarrow O^{2-}\ (ads) \quad (4)$$

A depletion region is created in the wall of Zn_2SnO_4 nanorods because electrons in the surface region of the Zn_2SnO_4 nanorods walls are consumed, resulting in a decrease in the electrical resistance of the Zn_2SnO_4 nanorods. The more oxygen ions are on the surface, the thicker the surface depletion layer, the higher the potential barrier, and the lower the electrical current.

Upon exposure to NO_2 gas, NO_2 gas adsorbs on the Zn_2SnO_4 nanorods and electrons are released from Zn_2SnO_4 nanorods, and are attracted to the adsorbed NO_2 molecules because an oxidizing gas, such as NO_2, acts as an electron acceptor, as shown in the following reactions [33]:

$$NO_2\ (g) + e^- \leftrightarrow NO_2^-\ (ads) \quad (1)$$

$$NO_2\ (g) + e^- \leftrightarrow NO\ (g) + O^-\ (ads) \quad (2)$$

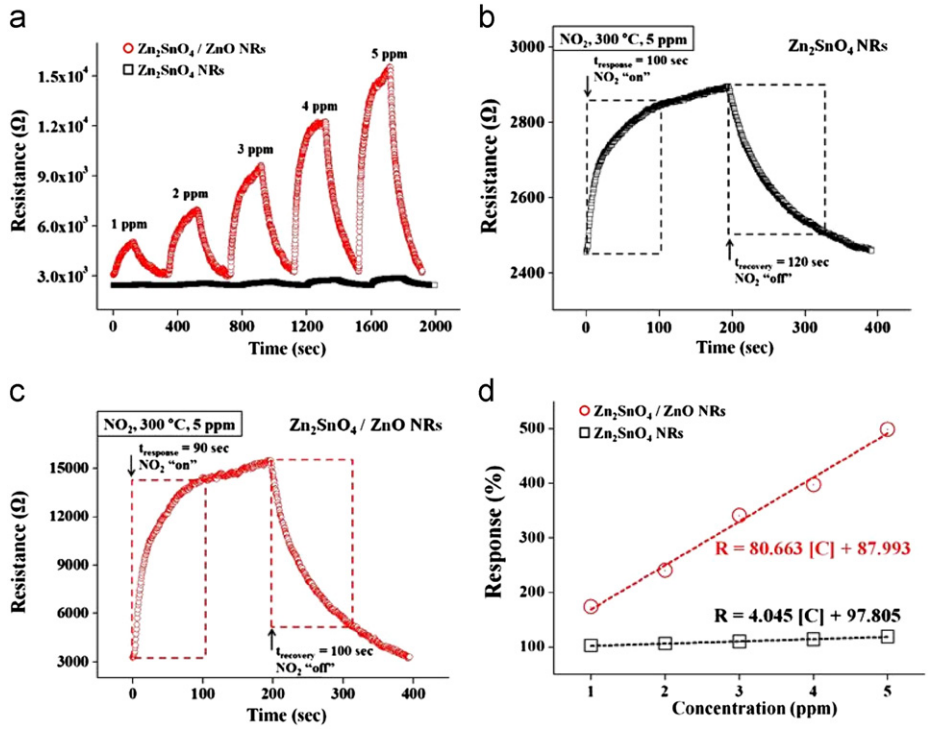

Fig. 6. Dynamic responses of (a) the Zn_2SnO_4 nanorod and Zn_2SnO_4-core/ZnO-shell nanorod gas sensors. (b) Enlarged part of (a) the Zn_2SnO_4 nanorod curve at 5 ppm NO_2. (c) Enlarged part of (a) Zn_2SnO_4-core/ZnO-shell nanorod curve at 5 ppm NO_2. (d) Responses of Zn_2SnO_4 nanorod and Zn_2SnO_4-core/ZnO-shell nanorod gas sensors as a function of the NO_2 gas concentration.

Table 1
Responses, response times and recovery times measured at different NO_2 concentrations for the Zn_2SnO_4-core/ZnO-shell nanorod sensor at 300 °C.

Response (%)				Response Time (sec)			Recovery Time (sec)		
NO_2 Conc.	Zn_2SnO_4	ZnO[30]	Zn_2SnO_4/ZnO	Zn_2SnO_4	ZnO[30]	Zn_2SnO_4/ZnO	Zn_2SnO_4	ZnO[30]	Zn_2SnO_4/ZnO
1 ppm	102.21	3.84	173.26	150	170	90	160	500	130
2 ppm	105.85		240.26	130		110	130		120
3 ppm	109.37		341.11	140		120	140		130
4 ppm	113.82		397.15	100		80	130		140
5 ppm	118.45	5.56	498.13	100	370	90	120	490	100

As a result of these reactions, a depletion region forms in the surface region of each Zn_2SnO_4 nanorods, resulting in an increase in the resistance of the nanorod sensor. After stopping the NO_2 gas supply however, the trapped electrons are released to the Zn_2SnO_4 nanorods by NO_2 gas, resulting in a decrease in the depletion layer width and resistance. This leads to an increase in carrier concentration in the Zn_2SnO_4 nanorods and a decrease in the surface depletion layer width. In other words, the removed electrons are returned to the conduction band, which results in a sharp decrease in electrical resistance in the Zn_2SnO_4 nanorod sensors. On the other hand, the substantial improvement in the response of the Zn_2SnO_4 nanorods to NO_2 gas by encapsulating them with Zn_2SnO_4 can be explained by the space-charge model [34, 35]. NO_2 is a strongly oxidizing gas. Upon exposure to NO_2 gas, the NO_2 gas is chemisorbed by the core-shell nanorod sensor and electrons are released from the ZnO shell layers, and attracted to the adsorbed NO_2 molecules because an oxidizing gas, such as NO_2 acts as an electron acceptor in the reaction. This reaction will result in an increase in depletion layer width (Fig. 7) and the resistance of the nanorod sensor. After stopping the supply of NO_2 gas, the trapped electrons are released to the ZnO shell layer by NO_2 gas leading to a decrease in the depletion layer width (Fig. 7) and resistance. Electron exchange between the surface states and the ZnO shell layer occurs within the surface layer excluding the depletion layer. The width of the surface layer is in the order of the Debye length λ_D, which can be expressed as follows [36,37]:

$$\lambda_D = \left(\frac{\varepsilon k T}{q^2} n_c\right)^{1/2} \quad (7)$$

where ε is the static dielectric constant ($=8.75\times8.85\times10^{-12}$ F/m in ZnO), k is the Boltzmann constant

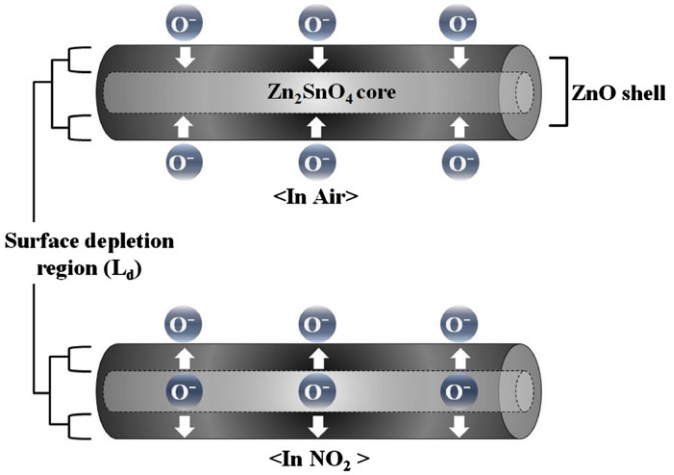

Fig. 7. Schematic diagram showing the width of the depletion region in a Zn_2SnO_4 nanorod upon exposure to air and NO_2 gas. The surface depletion layer width (L_d) is larger than the ZnO shell layer thickness.

($=1.38\times10^{-23}$ J/K), T is the absolute temperature ($=573$ K), q is the electrical charge of the carrier ($=1.6\times10^{-19}$ C) and n_c is the carrier concentration ($=5.1\times10^{16}/cm^3$: the value obtained by Hall measurements of the ZnO thin film prepared on the Si (100) substrate by ALD). For the ZnO layer in the core-shell nanorods fabricated in this study, the calculated λ_D value for 300 °C was approximately 21.7 nm. This means that NO_2 molecules not only deplete the electrons in the ZnO shell layer, the width of which can be as small as approximately 20 nm, but also take electrons from the Zn_2SnO_4 core, as shown in Fig. 7. Therefore, in Zn_2SnO_4-core/ZnO-shell nanorods, the heterojunction barrier at the interface of the core and shell should also be considered because electron transport is modulated by the heterojunction. The conductivity, σ, can be expressed as follows [38]:

$$\sigma = \sigma_0 \exp\left(-\Phi_{eff}/kT\right), \tag{8}$$

where σ_0 is a constant, Φ_{eff} the effective energy barrier at the heterojunction, k a Boltzmann constant and T the absolute temperature. Upon exposure to NO_2 gas, Φ_{eff} will increase because NO_2 gas is adsorbed by the core-shell nanorod and electrons are attracted to the adsorbed NO_2 molecules. Consequently, either the conductivity of the core-shell nanorod decreases or the resistivity increases. On the other hand, after stopping the NO_2 gas supply, the electrons trapped by the adsorbed NO_2 molecules will be released and then trapped not only by the ZnO shell layer but also by the Zn_2SnO_4 core via the heterojunction. Φ_{eff} will decrease because the trapped electrons will return to the conduction bands of ZnO. Consequently, either the conductivity of the core-shell nanorod will increase or the resistivity will decrease. Therefore, electron transport is modulated by the heterojunction with an adjustable energy barrier height. In other words, the heterojunction acts as a lever in electron transfer by which the electron transfer is facilitated or restrained, resulting in enhanced sensing properties of the core-shell nanorod sensor.

4. Conclusions

Zn_2SnO_4-core/ZnO-shell nanorods were synthesized using a two-step process: the synthesis of Zn_2SnO_4 nanorods by the thermal evaporation of a mixture of ZnO, SnO_2 and graphite powders (2: 1: 3 wt%) followed by the atomic layer deposition (ALD) of ZnO. The nanorods were a few tens to a few hundreds of nanometers in diameter and up to a few micrometers in length. The cores and shells of the nanorods were single crystal Zn_2SnO_4 and single crystal ZnO, respectively. Multiple networked Zn_2SnO_4 nanorods showed responses of approximately 102, 106, 109, 114 and 118% at NO_2 concentrations of 1, 2, 3, 4 and 5 ppm, respectively (Table 1). The responses of the Zn_2SnO_4 nanorods were significantly (~26 and ~21 fold) higher than those of the ZnO nanowires at 1 and 5 ppm NO_2, respectively. In contrast, the Zn_2SnO_4-core/ZnO-shell nanorods showed responses of 173, 240, 341, 397 and 498% at NO_2 concentrations of 1, 2, 3, 4 and 5 ppm, respectively (Table 1). Therefore, the response of the nanorods was improved 2–5 fold at each NO_2 concentration by the encapsulation of Zn_2SnO_4 nanorods with ZnO, and was ~45 and ~90 fold higher than ZnO nanowires at NO_2 concentrations of 1 and 5 ppm, respectively. The substantial improvement in the response of the Zn_2SnO_4 nanorods to NO_2 gas by the encapsulation of them by ZnO can be explained by the space-charge model. The Zn_2SnO_4-ZnO heterojunction acts as a lever in electron transfer through which electron transfer is facilitated or restrained, resulting in enhanced sensing properties of the core-shell nanorod sensor.

Acknowledgment

This study was supported by 2010 Core Research Program through the National Research Foundation of Korea (NRF) funded by the Ministry of Education, Science and Technology.

References

[1] H.H. Tippins, Optical absorption and photoconductivity in the band edge of b-Ga_2O_3, Physical Review A 140 (1965) 316–319.
[2] H. Kim, C. Jin, S. Park, S. Kim, C. Lee, H_2S gas sensing properties of bare and Pd-functionalized CuO nanorods, Sensors and Actuators, B 161 (2012) 594–599.
[3] D.H. Yoon, J.H. Yu, G.M. Choi, CO gas sensing properties of ZnO–CuO composite, Sensors and Actuators, B 46 (1998) 15–23.
[4] J.H. Yu, G.M. Choi, Electrical and CO gas sensing properties of ZnO–SnO_2 composites, Sensors and Actuators, B 52 (1998) 251–256.
[5] H.Y. Bae, G.M. Choi, Electrical and reducing gas sensing properties of ZnO and ZnO–CuO thin films fabricated by spin coating method, Sensors and Actuators, B 55 (1999) 47–54.
[6] J.H. Yu, G.M. Choi, Electrical and CO gas-sensing properties of ZnO/SnO_2 hetero-contact, Sensors and Actuators, B 61 (1999) 59–67.
[7] J.D. Choi, G.M. Choi, Electrical and CO gas sensing properties of layered ZnO–CuO sensor, Sensors and Actuators, B 69 (2000) 120–126.

[8] J.H. Yu, G.M. Choi, Current–voltage characteristics and selective CO detection of Zn_2SnO_4 and ZnO/Zn_2SnO_4, SnO_2/Zn_2SnO_4 layered-type sensors, Sensors and Actuators, B 72 (2001) 141–148.
[9] T. Lana-Villarreal, G. Boschloo, A. Hagfeldt, Nanostructured zinc stannate as semiconductor working electrodes for dye-sensitized solar cells, Journal of Physical Chemistry C 111 (2007) 5549–5556.
[10] M. Miyauchi, Z. Liu, Z.G. Zhao, S. An, K. Hara, Single crystalline zinc stannate nanoparticles for efficient photo-electrochemical devices, Chemical Communications 46 (2010) 1529–1531.
[11] B. Tan, E. Toman, Y. Li, Y. Wu, Zinc stannate (Zn_2SnO_4) dye-sensitized solar cells, Journal of the American Chemical Society 129 (2007) 4162–4163.
[12] I. Stambolova, K. Konstantinov, D. Kovacheva, P. Peshev, T. Donchev, Spray pyrolysis preparation and humidity sensing characteristics of spinel zinc stannate thin films, Journal of Solid State Chemistry 128 (1997) 305–309.
[13] D. Chen, J. Xu, B. Liang, X. Wang, P.C. Chen, C. Zhou, G. Shen, Electric transport, reversible wettability and chemical sensing of single-crystalline zigzag Zn_2SnO_4 nanowires, Journal of Materials Chemistry 21 (2011) 17236–17241.
[14] Y.J. Chen, X.Y. Xue, Y.G. Wang, T.H. Wang, Synthesis and ethanol sensing characteristics of single crystalline SnO_2 nanorods, Applied Physics Letters 87 (233503) (2005) 1–3.
[15] F. Pourfayaz, Y. Mortazavi, A. Khodadadi, S. Ajami, Ceria-doped SnO_2 sensor highly selective to ethanol in humid air, Sensors and Actuators B 130 (2008) 625–629.
[16] N. Hiratsuka, A. Hosoi, H. Kobayashi, K. Kakizaki, Isobutane gas sensing characteristics of zinc–tin complex oxide system, Journal of the Ceramic Society of Japan (International Edition) 104 (1996) 1173–1175.
[17] I. Stambolova, K. Konstantinov, M. Khristova, P Peshev, NO sensitivity of spinel type Zn_2SnO_4 spray deposited films, Physica Status Solidi (a) 167 (1998) R11–R12.
[18] S. Matsushima, S. Kunitsugu, K. Kobayashi, G. Okada, NO_2 sensing properties of thick Zn_2SnO_4 film, Journal of the Ceramic Society of Japan 103 (1995) 302–303.
[19] H. Nanto, T. Morita, H. Habara, K. Kondo, Y. Douguchi, T. Minami, Doping effect of SnO_2 on gas sensing characteristics of sputtered ZnO thin film chemical sensor, Sensors and Actuators, B 36 (1996) 384–387.
[20] J.H. Yu, G.M. Choi, Selective CO gas detection of Zn_2SnO_4 gas sensor, Journal of Electroceramics 8 (2002) 249–255.
[21] J. Zhang, X. Liu, L. Wang, T. Yang, X. Guo, S. Wu, S. Wang, S. Zhang, Synthesis and gas sensing properties of α-Fe_2O_3@ZnO core-shell nanospindles, Nanotechnology 22 (2011) 185501–185507.
[22] X. Liu, J. Zhang, X. Guo, S. Wang, S. Wu, Core-shell α-Fe_2O_3@SnO_2/Au hybrid structures and their enhanced gas sensing properties, RSC Advances 2 (2012) 1650–1655.
[23] M.A. Sanchez-Castillo, C. Couto, W.B. Kim, J.A. Dumestic, Gold-nanotube membranes for the oxidation of CO at gas–water interfaces, Angewandte Chemie 116 (2004) 1160–1162.
[24] G. Jágerszki, R.E. Gyurcsányi, L. Höfler, E. Pretsch, Hybridization-modulated ion fluxes through peptide–nucleic-acid-functionalized gold nanotubes, A New Approach to Quantitative Label-Free DNA Analysis, Nano Letters 7 (2007) 1609–1612.
[25] Y. Oshima, A. Onga, Helical gold nanotube synthesized at 150 K, Physical Review Letter 91 (2003) 205503.
[26] S. Park, S. An, H. Ko, C. Jin, C. Lee, Synthesis of nanograined ZnO nanowires and their enhanced gas sensing properties, ACS Applied Materials and Interfaces 4 (2012) 3650–3656.
[27] P. Feng, Q. Wan, T.H. Wang, Contact-controlled sensing properties of flowerlike ZnO nanostructures, Applied Physics Letters 87 (2005) 213111–213113.
[28] K.D. Schierbaum, U. Weimar, W. Goepel, R. Kowalkowski, Conductance, work function and catalytic activity of SnO_2-based gas sensors, Sensors and Actuators B 3 (1991) 205–214.
[29] O.V. Safonova, G. Delabouglise, B. Chenevier, A.M. Gaskov, M. Labeau, Co and NO_2 gas sensitivity of nanocrystalline tin dioxide thin films doped with Pd, Ru and Rh, Materials Science and Engineering C21 (2002) 105–111.
[30] C. Xu, J. Tamaki, N. Miura, N. Yamazoe, Grain size effects on gas sensitivity of porous SnO_2-based elements, Sensors and Actuators B 3 (1991) 147–155.
[31] C.L. Zhu, Y.J. Chen, R.X. Wang, L.J. Wang, M.S. Cao, X.L. Shi, Synthesis and enhanced ethanol sensing properties of α-Fe_2O_3/ZnO heteronanostructures, Sensors and Actuators, B 140 (2009) 185–189.
[32] H. Ogawa, M. Nishikawa, A. Abe, Hall measurement studies and an electrical conduction model of tin oxide ultrafine particle films, Journal of Applied Physics 53 (1982) 4448–4455.
[33] N. Barsan, U. Weimar, Conduction model of metal oxide gas sensors, Journal of Electroceramics 7 (2001) 143–167.
[34] C. Xu, J. Tamaki, N. Miura, N. Yamazoe, Grain size effects on gas sensitivity of porous SnO_2-based elements, Sensors and Actuators B 3 (1991) 147–155.
[35] C.L. Zhu, Y.J. Chen, R.X. Wang, L.J. Wang, M.S. Cao, X.L. Shi, Synthesis and enhanced ethanol sensing properties of α-Fe_2O_3/ZnO heteronanostructures, Sensors and Actuators B 140 (2009) 185–189.
[36] H. Ogawa, M. Nishikawa, A.J. Abe, Hall measurement studies and an electrical conduction model of tin oxide ultrafine particle films, Applied Physics 53 (1982) 4448–4455.
[37] N. Barsan, U.J. Weimar, Conduction model of metal oxide gas sensors, Electroceramics 7 (2001) 143–167.
[38] T. Weis, R. Lipperheide, U. Wille, S. Brehme, Barrier-controlled carrier transport in microcrystalline semiconducting materials: Description within a unified model, Journal of Applied Physics 92 (2002) 1411–1418.